JOC The Journal of Organic Chemistry

Article

pubs.acs.org/joc

Fluoreno[2,3-*b*]fluorene vs Indeno[2,1-*b*]fluorene: Unusual Relationship between the Number of π Electrons and Excitation Energy in *m*-Quinodimethane-Type Singlet Diradicaloids

Hirokazu Miyoshi,[†] Masahito Miki,[†] Shintaro Hirano,[†] Akihiro Shimizu,[†,#] Ryohei Kishi,[‡] Kotaro Fukuda,[‡] Daisuke Shiomi,[§] Kazunobu Sato,[§] Takeji Takui,[§] Ichiro Hisaki,[∥] Masayoshi Nakano,*[,‡,⊥] and Yoshito Tobe*[,†,⊥]

[†]Division of Frontier Materials Science, Graduate School of Engineering Science, [‡]Department of Materials Engineering Science, Graduate School of Engineering Science, and [⊥]Center for Spintronics Research Network (CSRN), Graduate School of Engineering Science, Osaka University, Toyonaka, Osaka 560-8531, Japan

[§]Department of Chemistry, Graduate School of Science, Osaka City University, Sumiyoshi-ku, Osaka 558-8585, Japan

[∥]Department of Material and Life Science, Graduate School of Engineering, Osaka University, Suita, Osaka 565-0871, Japan

Supporting Information

ABSTRACT: The dimesityl derivative of fluoreno[2,3-*b*]fluorene (**6b**) was synthesized and its structure and physical properties were investigated to elucidate the effects of its enhanced open-shell character, which was predicted theoretically in comparison with the smaller congener indeno[2,1-*b*]fluorene (**5b**). All structural and physical properties are in accordance with the theoretical predictions and can be interpreted in terms of the resonance contributors. The most remarkable spectroscopic property is the larger excitation energy of 24π-electron hydrocarbon **6b** than that of 20π-electron system **5b** in their lowest energy absorption bands of electronic spectra, a trend that is contrary to the well-known feature for common, alternant aromatic hydrocarbons. The theoretical basis of this unusual behavior was elucidated on the basis of the balance between the diradical character, exchange integral, and HOMO−LUMO gap and was confirmed by a complete-active-space configuration−interaction method with two electrons in two orbitals for the corresponding parent hydrocarbons **5a** and **6a**.

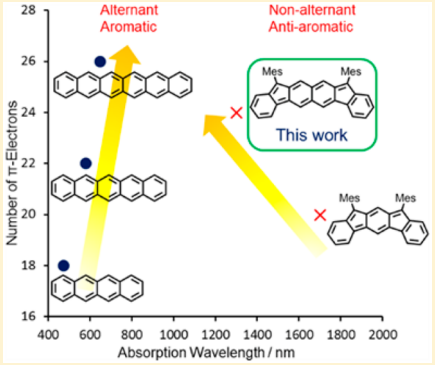

INTRODUCTION

Among polycyclic aromatic hydrocarbons (PAHs) that have been extensively studied in connection with their optoelectronic applications,[1] open-shell singlet diradicaloids have attracted a keen interest in view of their unique physical properties and potential applications for organic electronics,[2] nonlinear optics,[3] molecular spintronics,[4] and organic photovoltaics based on singlet fission,[5] associated with their weakly bonded π electrons.[6] Successful synthesis and characterization of inherently reactive molecules by attaching bulky substituents (kinetic stabilization) or annelating π systems which delocalize unpaired electrons (thermodynamic stabilization), combined with theoretical studies to treat with significantly correlated electronic states, and assessment of structural, physical, and materials properties have led to significant advances during the past decade. The majority of the singlet diradicaloids thus far synthesized contain a *p*-quinodimethane (*p*-QDM) unit, as represented by bisphenalenyls (**1**),[7] zethrenes (**2**),[8] and indeno[1,2-*b*]fluorene (**3a**),[9] or an isomeric *o*-quinodimethane (*o*-QDM) substructure as in indeno[2,1-*a*]fluorene (**4a**) (Figure 1).[10] Because of the dominant closed-shell character of *p*-QDM and *o*-QDM,[11] extension of π conjugation was conducted to increase open-shell character either by inserting additional cyclohexadiene units in the center of the π-framework, as exemplified by the congeners of **1**, **2**, and **4**,[12−14] or doubling the indenofluorene structures.[15] Recently, the increasing open-shell character by the former approach was theoretically analyzed in detail for indeno[1,2-*b*]fluorene (**3a**)[16] and its larger congener fluoreno[3,2-*b*]fluorene (**3b**) and was proven experimentally with a derivative of even larger congener diindeno[1,2-*b*:1′,2′-*i*]anthracene (**3c**).[17]

Contrary to singlet diradicaloids incorporating a *p*- or *o*-QDM unit, those with an embedded *m*-quinodimethane (*m*-QDM) unit are scarcely known because of their enhanced open-shell character due to the *m*-QDM unit, which has a triplet ground state.[11,18] In fact, indeno[2,1-*b*]fluorene derivative **5b** is the first and only known diradicaloid bearing a *m*-QDM unit in its π-framework.[19] The parent molecule **5a** is theoretically predicted to have significant open-shell character (y = 0.645, LC-UB3LYP/6-311+G**//UB3LYP/6-311+G** level)[16] and was proven crystallographically by the long bond

Received: October 13, 2016
Published: January 6, 2017

DOI: 10.1021/acs.joc.6b02500
J. Org. Chem. 2017, 82, 1380−1388

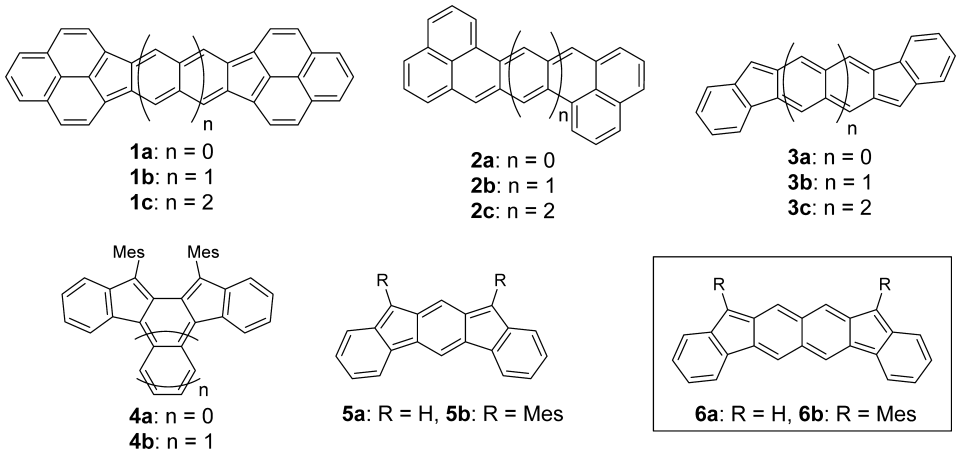

Figure 1. Chemical structure of bisphanalenes (**1**), zethrenes (**2**), and indenofluorenes **3**–**6** (Mes = 2,4,6-trimethylphenyl group).

Scheme 1. Resonance Structures of (a) Indeno[1,2-*b*]fluorene (3a), (b) Indeno[2,1-*b*]fluorene (5a), and (c) Fluoreno[2,3-*b*]fluorene (6a)

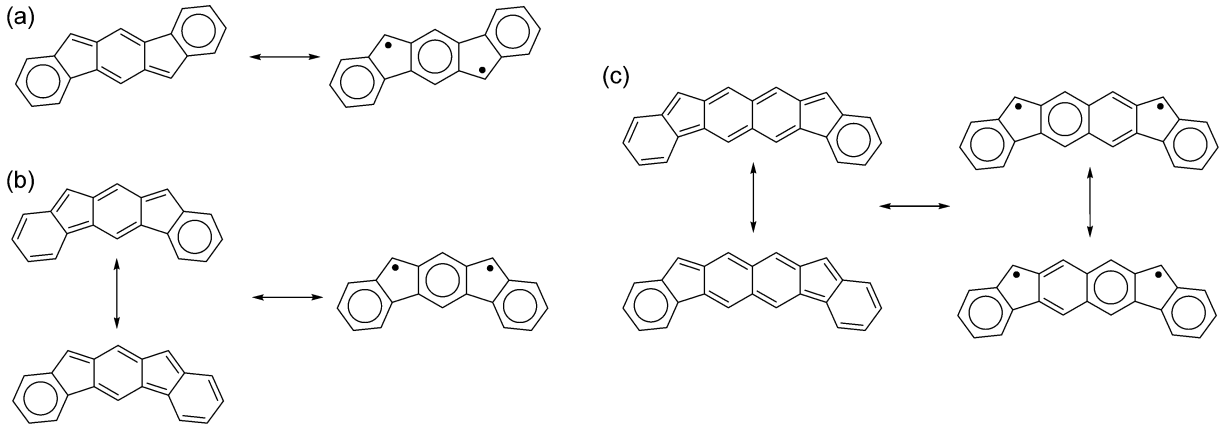

Scheme 2. Synthesis of 6b[a]

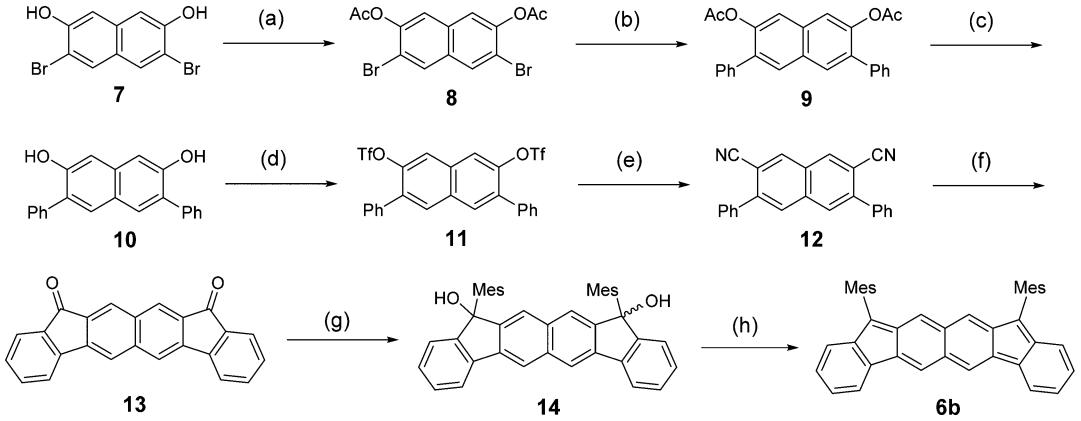

[a]Reagents and conditions: (a) Ac_2O, triethylamine, CH_2Cl_2, rt, 91%; (b) $PhB(OH)_2$, $Pd(PPh_3)_4$, Na_2CO_3, toluene, EtOH, H_2O, reflux, 89%; (c) NaOAc, EtOH, reflux, 94%; (d) Tf_2O, triethylamine, CH_2Cl_2, 0 °C → rt, 82%; (e) KCN, $Pd_2(dba)_3$·$CHCl_3$, DPPF, MeCN, 50 °C, 94%; (f) (i) NaOH, ethylene glycol, reflux, (ii) H_2SO_4, rt, 90% (two steps); (g) MesMgBr, Et_2O, rt, 80%; (h) $SnCl_2$, toluene, rt, 64%.

lengths around the five-membered ring and spectroscopically by the presence of the thermally accessible low-lying triplet state.[19] The larger open-shell character of **5a** compared to **3a** can also be interpreted by the resonance structures in which the closed-shell contributor has only one aromatic sextet for **5a** in contrast to that of **3a**, which has two sextets (Scheme 1a,b). Nevertheless, the central benzene ring is still involved significantly in π conjugation with the external benzene rings as judged from aromaticity (magnetic shielding tensor map) and odd electron density distribution.[16] Extension of π conjugation by replacing the benzene ring to naphthalene leads to fluoreno[2,3-*b*]fluorene (**6a**), which is predicted to exhibit increased open-shell character (y = 0.772) due to disconnection of π conjugation between the central naph-

DOI: 10.1021/acs.joc.6b02500
J. Org. Chem. 2017, 82, 1380−1388

thalene and external benzene units, localizing odd electron densities on the apical positions of the five-membered rings (Scheme 1c). To prove this aromaticity view of open-shell character experimentally by crystallographic and spectroscopic methods, we conducted the synthesis of dimesityl derivative **6b**. Most interestingly, an unusual phenomenon in the electronic transition of **6b** compared to **5b** was observed; the larger 24π system **6b** exhibits the lowest energy transition at 1293 nm, whereas the corresponding band of the smaller 20π compound **5b** appears at 1700 nm.[19] The theoretical basis for this unconventional behavior, which turned out to be specific to open-shell singlet molecules with moderate diradical character, is elucidated.

RESULTS AND DISCUSSION

Synthesis. The synthesis of **6b** was carried out starting from the known dibromonaphthalenediol **7**[20] as shown in Scheme 2. Acetylation of the hydroxyl group of **7** by acetic acid anhydride gave diacetate **8** in 91% yield. Suzuki–Miyaura cross-coupling between **8** and phenylboronic acid yielded diphenyl diacetate **9** in 89% yield. Hydrolysis of **9** by sodium acetate gave diol **10** in 94% yield. Diol **10** was treated with trifluoromethanesulfonic anhydride to afford ditriflate **11** in 82% yield. Palladium-catalyzed cyanation[21] of **11** was conducted to give dicyanide **12** in 94% yield. Hydrolysis followed by intramolecular Friedel–Crafts reaction gave diketone **13**. Addition of mesitylmagnesium bromide to **13** gave the corresponding diol **14** in 80% yield as a mixture of diastereomers in a ratio of 3:1; their stereochemistry was not determined. Dehydroxylation of **14** with tin(II) chloride gave **6b** as a green solid. Because **6b** readily decomposed during chromatography on deactivated silica gel or alumina, it was isolated by recrystallization after passing through a short column of deactivated alumina under an Ar flow. Compound **6b** turned out to be less stable than **5b**; it decomposed within 18 h in solution under ambient conditions (Figure S6, SI) in contrast to **5b**, whose half-life was determined to be about 30 h under similar conditions.[19] This result is consistent with the larger open-shell character of the singlet ground state **6b** than that of **5b** and the low-lying triplet state of **6b**.

Molecular Structure. Crystals suitable for X-ray structure analysis were obtained by recrystallization from benzene solution with slow diffusion of MeOH. The bond lengths of the π-framework of **6b** are listed in Table 1 (bond numbering, Figure 3) together with the theoretical values for **6a**[16] and those of the crystallographic structure **5b**.[19] As shown in Figure 2, the fluorenofluorene core of **6b** adopts a planar geometry with deviations from the mean square plane less than 0.157 Å. The two mesityl groups are nearly orthogonal to the backbone with dihedral angles of 88.40° and 69.78°. The bond lengths of the fluorenofluorene core are well reproduced by DFT calculations (UB3LYP/6-311+G** level).[16] The larger diradical character of **6b** is reflected in the bond length alternation of the fluorenofluorene core. For the five-membered rings, whereas the lengths of the most critical bonds *a* (1.437(2) Å) and *b* (1.424(2) Å) of **6b** are identical to those of **5b** (1.437(2) Å and 1.420(2) Å, respectively), bond *c* of **6b** (1.430(2) Å) is shorter than that of **5b** (1.438(2) Å). In order to evaluate the bond length alternation, the harmonic oscillator model of aromaticity (HOMA)[22] is used (Figure 3). The HOMA value of the outer benzene rings in **6b** (0.88) is slightly larger than those of **5b** (0.83), indicating that the outer benzene rings of **6b** have a more benzene-like structure. The central naphthalene ring of

Table 1. Experimental and Calculated Bond Lengths (Å) of the π-Framework of Indeno[2,1-*b*]fluorene (5b) and Fluoreno[2,3-*b*]fluorene (6a and 6b)

	X-ray[b]		calcd
bond[a]	**5b**[19]	**6b**	**6a**[16]
a	1.437 (2)	1.437 (2)	1.426
b	1.420 (2)	1.424 (2)	1.422
c	1.438 (2)	1.430 (2)	1.437
d	1.442 (2)	1.445 (2)	1.454
e	1.438 (2)	1.448 (2)	1.449
f	1.412 (2)	1.413 (2)	1.408
g	1.379 (2)	1.377 (2)	1.387
h	1.412 (2)	1.403 (3)	1.407
i	1.384 (2)	1.383 (2)	1.395
j	1.401 (2)	1.393 (2)	1.393
k	1.394 (2)	1.386 (2)	1.386
l	1.396 (2)	1.370 (2)	1.374
m	*c*	1.412 (2)	1.420
n	*c*	1.443 (2)	1.444
o	*c*	1.417 (2)	1.417

[a]Bond positions are shown in Figure 3. [b]Mean value. [c]Not applicable.

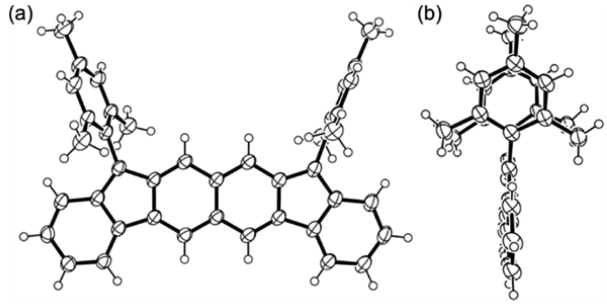

Figure 2. Crystal structure of **6b**. (a) Top view and (b) side view of the crystal structure. Ellipsoids drawn at 50% probability level. Solent molecules are omitted for clarity.

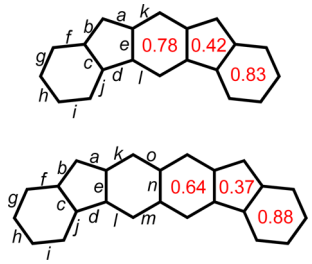

Figure 3. HOMA values of the π-frameworks of **5b** (top) and **6b** (bottom).

6b adopts a naphthalene-like structure[23] rather than a 2,7-naphthoquinodimethane in which the bonds *k* (1.387 (2) Å) and *l* (1.370 (2) Å) are relatively shorter than the bonds *m* (1.412 (2) Å) and *o* (1.417 (2) Å). The HOMA value of the central six-membered ring of **5b** (0.78), which is significantly smaller than that of benzene (0.98),[22] indicates its reduced aromatic character due to conjugation with the external benzene rings through the radical centers. On the other hand, the difference between the HOMA value of **6b** (0.64) from that of naphthalene (0.80)[22] is smaller, meaning that the radical centers on the five-membered rings do not participate as much in conjugation with the central 10π system. In other words, the singlet diradical canonical structure contributes

DOI: 10.1021/acs.joc.6b02500
J. Org. Chem. 2017, 82, 1380–1388

significantly in **6b**, thereby making **6b** exhibit larger open-shell character than **5b**. This is consistent with not only the magnetic tensor map[16] in which **6a** has a larger negative value for six-membered rings compared to **5a** but also the NICS(1) values[24] at the terminal benzene rings of **6a** (−4.81) and **5a** (−1.24) at the UB3LYP/6-311+G* level (Table S2, SI).

Physical Properties. In the ^{1}H NMR spectrum in CD_2Cl_2 **6b** did not show signals at 303 K (Figure 4 and Figures S2 and S3). By cooling to 193 K, only rather broad signals were observed at around 7 and 2 ppm due to aromatic and methyl protons, respectively. Similar behavior was also observed for **5b**; however, in the case of **5b** sharper signals were observed at low temperature.[19] This result indicates that the ground state of **6b** is singlet but the population of thermally excited triplet state is larger than that of **5b** at room temperature due to smaller singlet−triplet (S−T) energy difference. This is consistent with the theoretically estimated absolute S−T gap (UB3LYP/6-311+G** level) of **6a** (−8.8 kJ/mol), which is smaller than that of **5a** (−13.3 kJ/mol). In addition, a toluene solution of **6b** at 333 K exhibited an ESR signal at g = 2.004 but without splitting or $\Delta M_s = \pm 2$ transitions due to a triplet species (Figure S4), in contrast to **5b**, which exhibits typical splitting due to a triplet species.[19] The signal intensity decreased as the temperature was lowered to 173 K, suggesting the signal is due to the thermally excited triplet state in accordance with the NMR spectra and theoretical predictions. The absence of the splitting and the $\Delta M_s = \pm 2$ transitions can be ascribed to the weak spin−spin dipole interaction within the molecule and the long-distance separation between the two radicals.[25] However, the possibility of contribution due to radical impurities, which dissociate/associate depending on temperature, cannot be ruled out. In order to evaluate the S−T gap of **6b** experimentally, superconducting quantum interfering device (SQUID) measurement for a powder sample was undertaken at 1.9−300 K (Figure 5). From the fitting to the Bleaney−Bowers equation,[26] the S−T gap was determined to be −1150 K (−9.6 kJ/mol), which agrees with the theoretical value. More importantly, the experimental S−T gap is much smaller than that of **5b** (−2120 K),[19] supporting the larger open-shell character of the fluorenofluorene system.

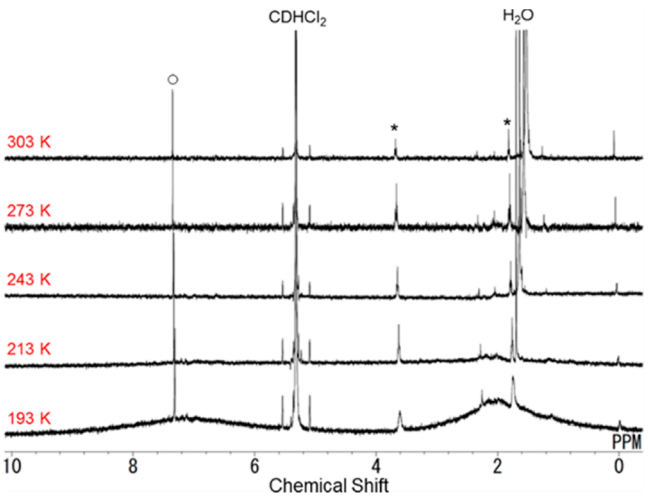

Figure 4. Variable-temperature ^{1}H NMR spectra of **6b** measured in a sealed tube in degassed CD_2Cl_2. Peaks labeled with a circle and asterisks are due to solvated benzene in crystals and THF left in a vacuum line, respectively.

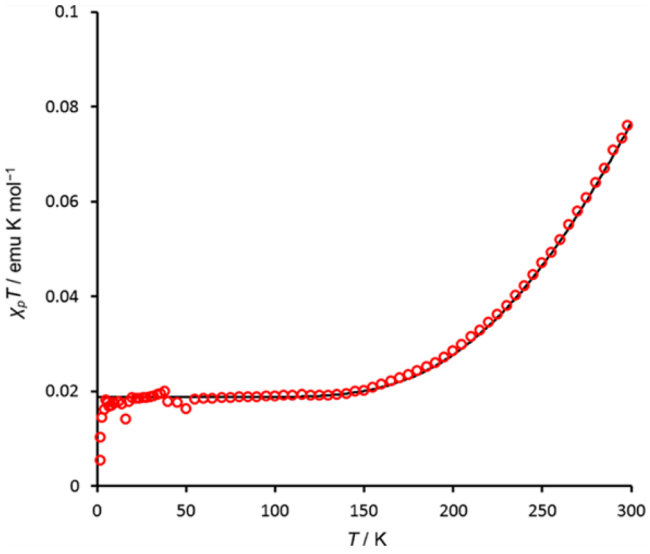

Figure 5. $\chi_p T-T$ plot of powder **6b**. The measured data are plotted as red circles. The black line is the theoretical curve calculated by using the Bleaney−Bowers equation with parameters of $2J/k_B$ = −1150 K, Curie impurity =5.0%, g = 2.00 (fixed), and diamagnetic susceptibility = -397×10^{-6} emu/mol.

As expected, the energy gap between the highest occupied molecular orbital (HOMO) and the lowest unoccupied molecular orbital (LUMO) of **6a** (1.10 eV) is predicted by DFT calculations (RB3LYP/6-311+G* level) to be smaller than that of **5a** (1.26 eV). The HOMO and LUMO energy levels are related to the first oxidation and the first reduction potentials measured by cyclic voltammetry.[27] The redox potentials and the relevant HOMO/LUMO energy levels of **6b** are listed in Table 2 together with those of **5b**,[19] *p*-QDM type indeno[1,2-*b*]fluorene derivative **3a-Mes**,[9c] and its homologue **3c-Mes** (see Figure 7 for the structures of **3a-Mes**, **3b-Mes**, and **3c-Mes**).[17] The theoretical HOMO/LUMO levels of the parent hydrocarbons **3a−c**, **5a**, and **6a** are also included. In the cyclic voltammogram (Figure 6), **6b** exhibited two reversible and two irreversible redox waves ($E_2^{ox,pa}$ = +0.66, E_1^{ox} = +0.00, E_1^{red} = −1.16, and $E_2^{red,pc}$ = −1.82 V vs Fc/Fc^+). The difference between the first oxidation and the first reduction potentials (ΔE_{redox}) of **6b** is determined to be 1.16 V, which is smaller than that of **5b** (1.26 V)[19] due to the lower oxidation potential of **6b**. This result is consistent with the theoretical prediction for **5a** and **6a**. When compared to the *p*-QDM-type indenofluorene derivatives **3a-Mes** and its homologue **3c-Mes**, the HOMO−LUMO energy gap of **5b** estimated by the redox potentials is much smaller than that of **3a-Mes** with the same number of π electrons. Although **3b-Mes**, a constitutional isomer of **6b**, has not been reported before, the theoretical HOMO−LUMO gap of **6a** as well as the experimental gap of **6b** are much smaller than the theoretical gap for **3b**. The HOMO−LUMO gaps of **6a** and **6b** are even smaller than the corresponding gaps of **3c** and **3c-Mes** with a larger number of π electrons (28π). These results reflect the larger diradical character of the *m*-QDM-type hydrocarbons than the *p*-QDM-type because with increasing open-shell character the HOMO−LUMO gap becomes smaller.

Excitation Energies of Lowest Energy Absorption Bands. The most remarkable spectroscopic feature in the *m*-QDM type nonalternant hydrocarbons **5b** and **6b** is their excitation energies of the lowest energy absorption bands in

DOI: 10.1021/acs.joc.6b02500
J. Org. Chem. 2017, 82, 1380−1388

Table 2. Computational[a] (3a, 3b, 3c, 5a, and 6a) and Experimental[b] (3a-Mes, 3c-Mes, 5b, and 6b) HOMO and LUMO Energy Levels[c]

p-quinodimethane type				*m*-quinodimethane type			
	HOMO (eV)	LUMO (eV)	H–L gap (eV)		HOMO (eV)	LUMO (eV)	H–L gap (eV)
3a	−5.51	−3.00	2.51	**5a**	−4.85	−3.58	1.28
3a-Mes	−5.34	−2.92	2.42	**5b**	−4.93	−3.67	1.26
3b	−5.09	−3.24	1.85	**6a**	−4.71	−3.61	1.10
3b-Mes[d]				**6b**	−4.80	−3.64	1.16
3c	−4.85	−3.33	1.52				
3c-Mes	−4.97	−3.52	1.45				

[a]The HOMO/LUMO levels of **3a**,[9b] **3b**,[16] **3c**,[17] **5a**,[16] and **6a**[16] were calculated at the RB3LYP6-311+G* level of theory for the molecular geometries reported in the respective reference. [b]Experimental HOMO and LUMO energy levels of **3a-Mes**, **3c-Mes**, **5b**, and **6b** were estimated by the redox potentials determined by CV. The values of **3c-Mes**,[17] **5b**,[19] and **6b** were calculated by using the reported potentials and the Fc/Fc^+ couple = −4.80 eV vs vacuum.[27] [c]Structures of **3a-Mes**, **3b-Mes**, and **3c-Mes** are shown in Figure 7. [d]Unknown.

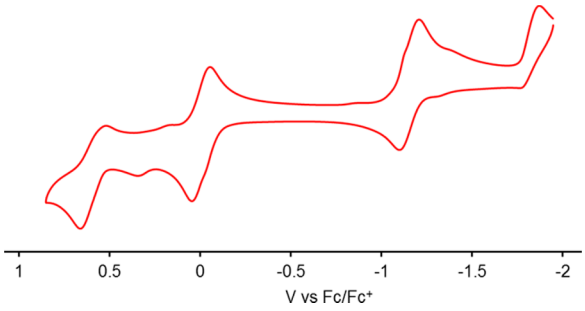

Figure 6. Cyclic voltammogram of **6b**. Conditions: in CH_2Cl_2 at room temperature, 0.1 M Bu_4NClO_4, working electrode: glassy carbon, counter electrode: Pt, reference electrode: $Ag/AgNO_3$, scan rate = 0.1 V/s.

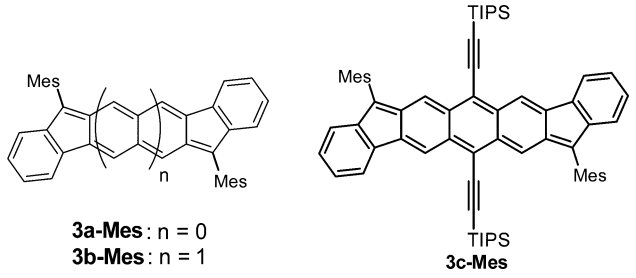

Figure 7. Chemical structures of **3a-Mes**, **3b-Mes**, and **3c-Mes**.

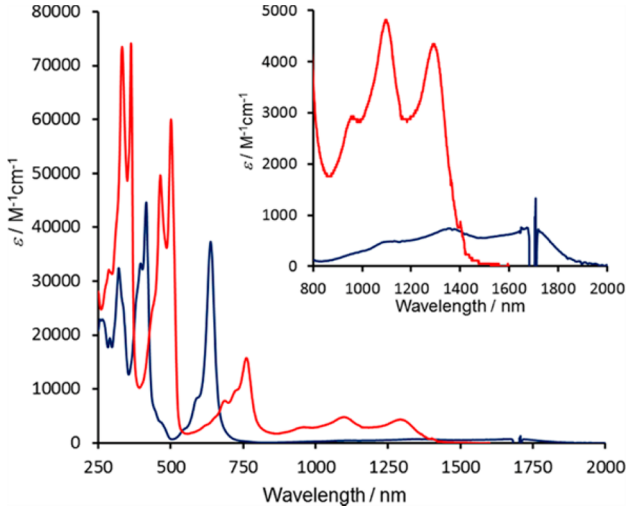

Figure 8. UV–vis–NIR absorption spectra of hydrocarbon **6b** (red) together with that of **5b**[19] (blue) in CH_2Cl_2 at room temperature. Inset: NIR region with expanded longitudinal axis. The discontinuity at around 1700 nm probably stems from the overtone of C–H vibration of the solvent.

electronic spectra. Figure 8 shows the absorption spectra for **6b** together with that of **5b**[19] for comparison in CH_2Cl_2. Compound **6b** exhibits an intense absorption band at 761 nm (ε = 15800) and a weak absorption band at 1293 nm (ε = 4350). The spectrum showed almost no change when cooled to 223 K, excluding the possibility of aggregation in solution. Similarly, polarity or the heavy atom[28] of solvents did not affect the absorption (Figure S5). These results exclude the possible effect of aggregation or singlet to triplet absorption[28] to the lowest energy absorption band, confirming that the lowest energy band is due to a π,π^* singlet-to-singlet excitation. This is consistent with a weak absorption at 1014 nm (f = 0.0618) predicted by TD-DFT calculations (UB3LYP/6-311+G** level). Interestingly, the lowest excitation band is shifted to shorter wavelength (i.e., larger excitation energy) compared to **5b** (1700 nm)[19] in the larger 24π-electron conjugation compared to the 20π-electron system **5b** in spite of the smaller HOMO–LUMO gap than that of **5a**. This trend is contrary to the commonly observed feature in alternant aromatic hydrocarbons such as for acenes[29] and rylenes[30] in which the larger π-system exhibits a lower energy for the first excitation band in a homologous series due to the smaller HOMO–LUMO gap.

To understand this phenomenon, we performed quantum chemical calculations. Here, we consider the first excitation energy E_{kg} as a function of diradical character y and other physical parameters based on the valence configuration interaction (VCI) analysis of the two-site diradical model with two electrons in two orbitals.[31] The E_{kg} is expressed as

$$E_{kg} = \frac{U}{2}\left[1 + \frac{1}{\sqrt{1-(1-y)^2}}\right] - 2K_{ab} = \frac{U}{2}f_E(y) - 2K_{ab} \quad (1)$$

where U is an effective Coulomb repulsion, K_{ab} is a direct exchange between the localized natural orbitals a and b ($\geq$0), and $f_E(y)$ indicates the square bracket part. The diradical character y is represented by

$$y = 1 - \frac{1}{\sqrt{1+\left(\frac{U}{4t_{ab}}\right)^2}} = 1 - \frac{1}{\sqrt{1+\left(\frac{K_{gu}^M}{\varepsilon_{ug}}\right)^2}} \quad (2)$$

where t_{ab} ($\leq$0) is a transfer integral in the localized natural orbital (LNO) basis. The second equality is obtained from the

DOI: 10.1021/acs.joc.6b02500
J. Org. Chem. 2017, 82, 1380–1388

relations $U = 2K_{gu}^{M}$ and $\varepsilon_{ug} = 2t_{ab}$, where K_{gu}^{M} and ε_{ug} indicate the exchange integral and the HOMO(g)−LUMO(u) gap ($\varepsilon_u - \varepsilon_g$) in the symmetry-adapted MO basis (g and u) representation, respectively. The diradical character indicates the effective bond weakness, or the degree of electron correlation, and takes a value between 0 (closed-shell) and 1 (pure diradical).[32] Also, we obtain the relationship

$$K_{ab} = \frac{1}{4}(J_{gg}^{M} + J_{uu}^{M} - 2J_{gu}^{M}) \quad (3)$$

where J_{ij}^{M} indicates the Coulomb repulsions between MOs i and j. On the basis of eq 1, we consider the dependence of E_{kg} on these physical parameters. Note that K_{ab} is definitely positive, so that larger K_{ab} leads to the decrease in E_{kg}.

First, let us consider nearly closed-shell systems ($y \sim 0$). As seen from eq 2, this is the case with $U \ll 4|t_{ab}|$. In this case, $f_E(y)$ in eq 1 becomes very large, but the prefactor $U/2$, which is a negligible value, attenuates the enhancement, and thus, the first term in eq 1 gives a finite value. Here, with keeping the y value, i.e., the ratio $|t_{ab}|/U$, the decrease of U (and $|t_{ab}|$) is found to contribute to the decrease of E_{kg}. In addition, the decrease of U (K_{gu}^{M}, i.e., the overlap between g and u) leads to the enhancement of K_{ab} since g and u tend to be distributed in mutually different spatial regions, resulting in $J_{gg}^{M} > J_{gu}^{M}$ and $J_{uu}^{M} > J_{gu}^{M}$ (see eq 3). As a result, if the y value of the system remains in the nearly closed-shell region, the decrease of $|t_{ab}|$ (HOMO−LUMO gap) and/or the decrease of K_{gu}^{M} (overlap between g and u) is found to be a possible way of reducing the first excitation energy E_{kg} (see eq 1). This is a conventional way of reducing the first excitation energy.

In addition, as seen from eq 1, there is another way of reducing E_{kg}, i.e., the increase of diradical character y. This case is realized when U (K_{gu}^{M}) is increased and $|t_{ab}|$ (HOMO−LUMO gap) is decreased. In such a case, the K_{ab} tends to decrease since the overlap between g and u becomes large; i.e., both distributions are in a similar region ($J_{gg}^{M} \sim J_{uu}^{M} \sim J_{gu}^{M}$) (see eq 3). Namely, the first excitation energy E_{kg} is shown to be governed by the first term (a function of U and y) in eq 1 and is predicted to decrease with increasing y until the moderate region by reflecting the y-dependent behavior of $f_E(y)$ (see Figure 9). On the other hand, further increase of the y value has a possibility of increasing E_{kg}. This is understood by the fact that the increase of y is associated with the increase of U (see eq 2), and $f_E(y)$ in eq 1 shows a rapid decrease in the relatively small y region ($y < \sim 0.2$) and subsequently reaches a stationary value. Namely, in the larger y region, the E_{kg} obtained by the product of $U/2$ and $f_E(y)$ is predicted to increase again due to the product of the large U and a nearly stationary value of $f_E(y)$. Since the extension of π-conjugation size tends to cause the increase of y due to the decrease of $|t_{ab}|$ as well as to the increase of U, this has a possibility of increasing E_{kg} for larger size π-conjugated systems with larger y values. This is contrary to the well-known feature.

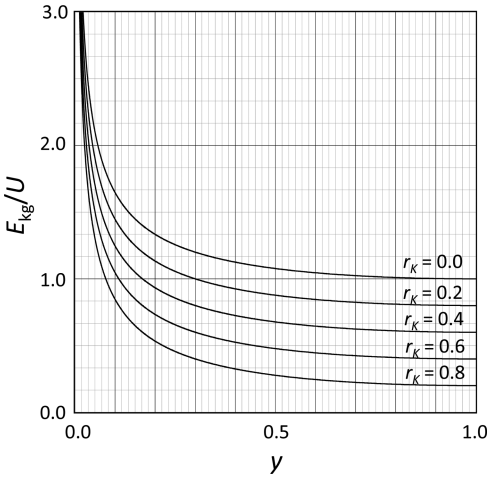

Figure 9. Diradical character dependence of dimensionless excitation energy E_{kg}/U for different $r_K = 2K_{ab}/U$ values (eq 1).

In order to confirm this prediction, we investigate the contribution of each physical parameter to E_{kg} of **5a** and **6a**, where **6a** exhibits larger E_{kg} than **5a** although **6a** has a larger π-conjugation size than **5a**. A complete-active-space configuration−interaction method with two electrons in two orbitals [CASCI(2,2)] was employed where the symmetry-adapted MOs, g and u, in the CAS space were obtained using the tuned long-range-corrected (LC)-BLYP method[33] with a range-separating parameter μ (= 0.202 bohr^{-1} for **5a** and 0.187 bohr^{-1} for **6a**), which has been optimized for each system so as to satisfy the exact condition (minus HOMO energy = vertical ionization potential) of density functional theory.[34,35] This CASCI(2,2) method qualitatively reproduces the first optically allowed excitation energies for condensed-ring systems (Figure S8). The calculated E_{kg} and each physical parameter are listed in Table 3. Apparently, **5a** and **6a** are found to be diradicaloids

Table 3. First Optically Allowed Excitation Energy (E_{kg}) and Each Physical Parameter Calculated by the CASCI(2,2) Method Using the Natural Orbitals (NOs) Obtained by Tuned-LC-RBLYP/6-31G* Calculation

	5a	6a
E_{kg} (au)	0.0972	0.1183
y (−)[a]	0.1797	0.3121
$\lvert t_{ab}\rvert$ (au)	0.0306	0.0260
$f_E(y)$ (−)	2.7483	2.3777
$\frac{U}{2} = K_{gu}^{M}$ (au)	0.0426	0.0550
$(U/2)f_E(y)$ (au)	0.1172	0.1307
J_{gg}^{M} (au)	0.1966	0.1710
J_{uu}^{M} (au)	0.1991	0.1788
J_{gu}^{M} (au)	0.1779	0.1625
$-2K_{ab}$ (au)	−0.0200	−0.0124

[a]Note that the theoretical occupation numbers of NOs, therefrom y is calculated, depend on the method of calculations.[36]

with y(**6a**) > y(**5a**), which is understood by the fact that $|t_{ab}|$ is smaller in **6a** than in **5a**, while U is larger in **6a** than in **5a**. As a result, $(U/2)f_E(y)$ is found to be larger in **6a** than in **5a**, although $f_E(y)$ is smaller in **6a** than in **5a**. Note here that $(U/2)f_E(y)$ is found to be a primary contribution to E_{kg} since $|-2K_{ab}|$ is shown to be much smaller than $(U/2)f_E(y)$ (and also holds the tendency that larger y value leads to smaller K_{ab} as predicted above: this also contributes to the relative decrease of E_{kg} in for smaller y value). These features substantiate the above prediction and demonstrate the feature that E_{kg} is reduced with increasing y value in the small y region, while a further increase of the y value, often caused by extension of the π-conjugation size, tends to increase the E_{kg} value again.

DOI: 10.1021/acs.joc.6b02500
J. Org. Chem. 2017, 82, 1380−1388

CONCLUSIONS

We have synthesized the dimesityl derivative of fluoreno[2,3-*b*]fluorene (**6b**) and investigated its structure and physical properties to compare the effects of its enhanced open-shell character predicted theoretically compared with the smaller congener indeno[2,1-*b*]fluorene (**5b**). The bond lengths determined by X-ray crystallographic analysis of **6b** indicate the location of larger spin densities in the apex positions of the five-membered rings of **6b** compared with **5b**. Temperature-dependent ^{1}H NMR and ESR spectra indicate the existence of a low-lying thermally excited triplet state as confirmed by SQUID measurement, which gives a smaller signet−triplet energy gap of −9.6 kJ/mol for **6b** than **5b**. The small HOMO−LUMO energy gap of **6b** was confirmed by cyclic voltammetry, which showed reversible first and second one-electron oxidation and reduction waves. The most remarkable spectroscopic feature of 24π-electron system **6b** is its larger excitation energy with a maximum at 1293 nm, which was shorter wavelength shifted than that of 20π-electron system **5b** (1700 nm). To clarify the reason for this unusual behavior, which is contrary to the commonly observed feature for alternant aromatic hydrocarbons, the theoretical analysis was carried out on the basis of the balance between the diradical character, exchange integral, and HOMO−LUMO gap. The analysis also suggests that such unusual behavior is a characteristic feature common in diradicaloids of moderate open-shell character. Finally the theoretical estimate was confirmed quantitatively by a CASCI-(2,2) method with two electrons in two orbitals for the corresponding parent hydrocarbons **5a** and **6a**.

EXPERIMENTAL SECTION

General Considerations. Melting points were measured with a hot-stage apparatus and are uncorrected. ^{1}H and ^{13}C NMR spectra were recorded on a spectrometer at 400 MHz for ^{1}H and 100 MHz for ^{13}C at 30 °C. When chloroform-*d*, dichlomethane-d_2, 1,1,2,2-tetrachloroethane-d_2, and toluene-d_8 were used as solvent, the spectra were referenced to residual solvent proton signals in the ^{1}H NMR spectra (7.26 ppm for chloroform-*d*, 5.32 ppm for dichlomethane-d_2, and 6.97 ppm for toluene-d_8) and to the solvent carbons in the ^{13}C NMR spectra (77.0 ppm for chloroform-*d*, and 73.78 ppm for 1,1,2,2-tetrachloroethane-d_2). ESR spectra were recorded in the temperature range of 173−333 K. IR spectra were recorded as KBr disks or via the Nujol method. Mass spectral analyses were performed with a FAB mode using an instrument employing a quadrupole doublet-based lens system with a resolution exceeding 60000. Cyclic voltammograms were recorded with a glassy carbon working electrode and Pt counter electrode in CH_2Cl_2 containing 0.1 M Bu_4NClO_4 as the supporting electrolyte. The experiments were performed by employing an Ag/$AgNO_3$ reference electrode at room temperature. The temperature-dependent magnetic susceptibility was measured for randomly oriented polycrystalline samples of **6b** with an applied field of 1 T in the temperature range of 1.9−300 K. Column chromatography and TLC were performed with silica gel 60 (70−230 mesh ASTM) and silica gel 60 F254, respectively. All reagents, except for 3,6-dibromo-2,7-naphthalenediol (**7**),[20] were obtained from commercial suppliers and used as received. Toluene was dried over CaH_2 and distilled prior to use. CH_2Cl_2 and Et_2O were dried by a Glass Contour solvent purification system. NICS calculations and TD-DFT calculations were performed using Gaussian 09, revision D.01.[37] The molecular geometries of **5a** and **6a** reported in a literature[16] were used. The theoretical chemical shifts were calculated by the GIAO-B3LYP method.

Materials Synthesis. *2,7-Diacetoxy-3,6-dibromonaphthalene (**8**).* To a solution of **7**[20] (8.63 g, 27.1 mmol) and Et_3N (20.0 mL, 143 mmol) in CH_2Cl_2 (350 mL) was added acetic anhydride (8.40 mL, 88.9 mmol) at 0 °C, and the reaction mixture was stirred at room temperature for 4 h. After addition of 1 M HCl, the mixture was extracted with CH_2Cl_2. The organic layer was washed with saturated aqueous $NaHCO_3$ solution and brine and dried over anhydrous $MgSO_4$. After evaporation of the solvent, column chromatography on silica gel (hexanes/EtOAc = 10/1) gave diacetate **8** (9.87 g, 91%) as a colorless solid: mp 159.0−160.0 °C; R_f = 0.57 (hexanes/EtOAc = 2/1); ^{1}H NMR (400 MHz, $CDCl_3$, 30 °C) δ 8.05 (s, 2H), 7.54 (s, 2H), 2.41 (s, 6H); ^{13}C NMR (100 MHz, $CDCl_3$, 30 °C) δ 168.5, 146.4, 132.1, 131.2, 131.1, 120.6, 116.3, 20.8; IR (KBr) 3069, 3023, 2987, 2937, 1759, 1590, 1484, 1437, 1407, 1369, 1359, 1209, 1196, 1146, 1019, 1001, 919, 854, 823, 685, 671, 632, 606 cm^{-1}; MS (FAB) *m*/*z* 402.9 [M$^+$]; HRMS (FAB) calcd for $C_{14}H_{10}O_4{}^{79}Br_2$ 399.8946, found 399.8947(M$^+$).

*2,7-Diacetoxy-3,6-diphenylnaphthalene (**9**).* Diacetate **8** (1.02 g, 2.54 mmol), Na_2CO_3 (581 mg, 5.48 mmol), and $PhB(OH)_2$ (732 mg, 6.00 mmol) were placed in a three-necked flask, and the flask was charged with Ar. After addition of toluene (80 mL), water (2.6 mL), and EtOH (2.6 mL), Ar was bubbled into the solution for 25 min. To this solution was added $Pd(PPh_3)_4$ (291 mg, 252 μmol), and the mixture was heated under reflux for 20 h before it was diluted with water and extracted with CH_2Cl_2. The extract was washed with brine and dried over anhydrous $MgSO_4$. After evaporation of the solvent, column chromatography on silica gel (hexanes/EtOAc = 9/1) gave **9** (893 mg, 89%) as a colorless solid: mp 152.0−152.5 °C; R_f = 0.57 (hexanes/EtOAc = 2/1); ^{1}H NMR (400 MHz, $CDCl_3$, 30 °C) δ 7.89 (s, 2H), 7.59 (s, 2H), 7.52−7.49 (m, 4H), 7.47−7.42 (m, 4H), 7.41−7.36 (m, 2H), 2.10 (s, 6H); ^{13}C NMR (100 MHz, $CDCl_3$, 30 °C) δ 169.3, 146.9, 137.5, 134.7, 132.9, 130.2, 129.9, 129.1, 128.3, 127.6, 119.5, 20.8; IR (KBr) 3053, 3026, 2935, 1764, 1748, 1486, 1413, 1366, 1229, 1200, 1178, 1131, 1032, 1011, 920, 768, 705, 698 cm^{-1}; MS (FAB) *m*/*z* 396.1 (M$^+$). Anal. Calcd for $C_{26}H_{20}O_4$: C, 78.77; H, 5.09. Found: C, 78.76; H, 5.02.

*2,7-Dihydroxy-3,6-diphenylnaphthalene (**10**).* Compound **9** (3.68 g, 9.29 mmol) was placed in a three-necked flask, and the flask was charged with Ar. After addition of EtOH (200 mL) and water (40 mL), Ar was bubbled into the solution for 30 min. To this solution was added sodium acetate (20.2 g, 247 mmol), and the mixture was heated under reflux for 116 h. After addition of water and concd HCl, the resulting precipitate was collected by filtration to give diol **10** (2.78 g, 94%) as a gray solid: mp 168.0−169.0 °C; R_f = 0.22 (hexanes/EtOAc = 2/1); ^{1}H NMR (400 MHz, $CDCl_3$, 30 °C) δ 7.67 (s, 2H), 7.56−7.50 (m, 8H), 7.45−7.42 (m, 2H), 7.22 (s, 2H), 5.27 (s, 2H); ^{13}C NMR (100 MHz, $CDCl_3$, 30 °C) δ 151.5, 137.0, 135.4, 129.5, 129.3, 129.2, 128.6, 128.0, 124.6, 108.7; IR (KBr) 3486, 3057, 3028, 1628, 1600, 1489, 1419, 1372, 1262, 1175, 1130, 1033, 911, 870, 903, 770, 701 cm^{-1}; MS (FAB) *m*/*z* 312.2 (M$^+$); HRMS (FAB) calcd for $C_{22}H_{16}O_2$ 312.1151, found 312.1146.

*2,7-Bis(trifluoromethylsulfonyl)-3,6-diphenylnaphthalene (**11**).* To a solution of **10** (2.77 g, 8.87 mmol) and Et_3N (10.0 mL, 71.7 mmol) in CH_2Cl_2 (100 mL) was added trifluoromethanesulfonic anhydride (6.00 mL, 35.7 mmol) at 0 °C under an argon atmosphere, and the solution was stirred at room temperature for 10 h. After addition of water and 1 M HCl, the mixture was extracted with $CHCl_3$. The organic layer was washed with saturated aqueous $NaHCO_3$ solution and brine and dried over anhydrous $MgSO_4$. After evaporation of the solvent, column chromatography on silica gel (hexanes/EtOAc = 20/1) gave ditriflate **11** (4.23 g, 82%) as a colorless solid: mp 140.5−141.8 °C; R_f = 0.78 (hexanes/EtOAc = 4/1); ^{1}H NMR (400 MHz, $CDCl_3$, 30 °C) δ 7.99 (s, 2H), 7.94 (s, 2H), 7.55−7.45 (m, 10H); ^{13}C NMR (100 MHz, $CDCl_3$, 30 °C) δ 146.2, 135.7, 135.1, 131.7, 131.5, 131.2, 129.6, 128.73, 128.65, 120.0, 118.3 (q, *J* = 319 Hz, CF_3); ^{19}F NMR (376 MHz, $CDCl_3$) δ − 74.9 (s); IR (KBr) 3070, 3058, 3032, 1488, 1421, 1408,1367, 1224, 1209, 1136, 1119, 1109, 1034, 880, 857, 816, 766, 700, 636, 614 cm^{-1}; MS (FAB) *m*/*z* 576.0 (M$^+$). Anal. Calcd for $C_{24}H_{14}F_6O_6S_2$: C, 50.00; H, 2.45. Found: C, 50.06; H, 2.10.

*2,7-Dicyano-3,6-diphenylnaphthalene (**12**).* Ditriflate **11** (2.53 g, 4.39 mmol), DPPF (723 mg, 1.30 mmol), and KCN (1.14 g, 17.5 mmol) were placed in a two-necked flask, and the flask was charged with Ar. After addition of MeCN (50 mL), Ar was bubbled into the

DOI: 10.1021/acs.joc.6b02500
J. Org. Chem. 2017, 82, 1380−1388

solution for 15 min. To this solution was added $Pd_2(dba)_3{\cdot}CHCl_3$ (367 mg, 355 μmol), and the mixture was heated at 50 °C for 5 h. The mixture was diluted with a buffer solution consisting of saturated aqueous NH_4Cl and concentrated aqueous ammonia (v/v = 4/1) and extracted with $CHCl_3$. The extract was washed with brine and dried over anhydrous $MgSO_4$. After evaporation of the solvent, column chromatography on silica gel (hexanes/$CHCl_3$ = 2/3) followed by recrystallization from a mixture of $CHCl_3$/hexane gave dicyanide **12** (1.38 g, 94%) as a colorless solid: mp 198.3−199.5 °C; R_f = 0.59 (hexanes/EtOAc = 4/1); ^{1}H NMR (400 MHz, $CDCl_3$, 30 °C) δ 8.44 (s, 2H), 8.01 (s, 2H), 7.67−7.65 (m, 4H), 7.58−7.49 (m, 6H); ^{13}C NMR (100 MHz, $CDCl_3$, 30 °C) δ 143.1, 137.4, 135.9, 135.8, 129.23, 129.19, 129.02, 128.95, 128.92, 117.9, 111.5; IR (KBr) 3051, 3022, 2227, 2220, 1627, 1577, 1480, 1456, 1448, 1355, 1078, 1002, 926, 902, 768, 696 cm^{-1}; MS (FAB) *m*/*z* 331.2 ([M + H]$^+$). Anal. Calcd for $C_{24}H_{14}N_2$: C, 87.25; H, 4.27; N, 8.48. Found: C, 86.98; H, 4.04; N, 8.50.

*11,14-Dihydrofluoreno[2,3-b]fluorene-11,14-dione (**13**).* To a solution of **12** (1.77 g, 5.36 mmol) in ethylene glycol (110 mL) was added NaOH (5.63 g, 140 mmol), and the solution was stirred under reflux for 16 h. After cooling, the reaction mixture was acidified by concd HCl, and the resulting precipitate was collected by filtration to give crude diacid (1.91 g). This material was added to concd H_2SO_4 (60 mL), and the mixture was stirred at room temperature for 4 h. The mixture was poured into ice, and the yellow precipitate was collected by filtration and washed with MeOH to give diketone **13** (1.60 g, 90%) as a yellow solid: mp 307 °C dec; R_f = 0.76 ($CHCl_3$/EtOAc = 9/1); ^{1}H NMR (400 MHz, $CDCl_3$, 30 °C) δ 8.21 (s, 2H), 7.91 (s, 2H), 7.80−7.75 (m, 4H), 7.61 (dd, *J* = 7.5, 7.5 Hz, 2H), 7.41 (dd, *J* = 7.5, 7.4 Hz, 2H); ^{13}C NMR (100 MHz, $C_2D_2Cl_4$, 80 °C) δ 191.7, 143.8, 141.7, 141.1, 136.1, 134.9, 134.0, 133.4, 129.8, 127.1, 124.4, 121.1, 119.5; IR (KBr) 3034, 2925, 2853, 1704, 1629, 1603, 1461, 1422, 1315, 1293, 1187, 1109, 996, 917, 875, 760, 720, 587 cm^{-1}; MS (FAB) *m*/*z* 333.1 ([M + H]$^+$); HRMS (FAB) calcd for $C_{24}H_{13}O_2$ 333.0915, found 333.0912 ([M + H]$^+$).

*11,14-Dimesityl-11,14-dihydrofluoreno[2,3-b]fluorene-11,14-diol (**14**).* To a solution of mesitylmagnesium bromide in ether freshly prepared from 2-bromomesitylene (599 mg, 3.01 mmol), 1,2-dibromoethane (1.08 g, 5.82 mmol), and magnesium (222 mg, 9.14 mg atom) in ether (14 mL) was added **13** (144 mg, 432 μmol) at room temperature under an argon atmosphere, and the solution was stirred for 4 h. After addition of water and 1 M HCl, the mixture was extracted with CH_2Cl_2. The organic layer was washed with saturated aqueous $NaHCO_3$ solution and brine, dried over anhydrous $MgSO_4$, and concentrated under reduced pressure. The residue was subjected to column chromatography on silica gel (hexanes/AcOEt = 8/1 → 5/1) to give diol **14** (199 mg, 80%) as a mixture of diastereomers with different polarity, whose R_f values in CH_2Cl_2 were 0.75 and 0.15. First diastereomer (58.1 mg, 23%): colorless solid; mp 270 °C dec; R_f = 0.75 (CH_2Cl_2); ^{1}H NMR (400 MHz, $CDCl_3$, 30 °C) δ 8.14 (s, 2H), 7.84 (d, *J* = 7.2 Hz, 2H), 7.60 (s, 2H), 7.43 (ddd, *J* = 7.4, 7.4, 1.2 Hz, 2H), 7.33−7.29 (m, 4H), 6.99 (s, 2H), 6.60 (s, 2H), 2.95 (s, 6H), 2.25 (s, 6H), 2.16 (s, 2H), 1.22 (s, 6H); ^{13}C NMR (100 MHz, $CDCl_3$, 30 °C) δ 151.6, 149.1, 138.8, 138.7, 138.5, 136.23, 136.18, 135.5, 135.0, 134.6, 132.3, 130.8, 129.3, 129.1, 124.3, 123.7, 120.9, 119.1, 85,9, 25.7, 21.6, 20.5; IR (KBr) 3555, 3527, 3011, 2970, 2938, 2920, 2859, 1632, 1609, 1566, 1492, 1478, 1450, 1432, 1379, 1326, 1290, 1200, 1154, 1138, 1118, 1045, 1010, 989, 930, 911, 882, 849, 785, 755, 702, 634 cm^{-1}; MS (FAB) *m*/*z* 572.3 (M$^+$); HRMS (FAB) calcd for $C_{42}H_{36}O_2$ 572.2717, found 572.2716 (M$^+$). Second diastereomer (141 mg, 57%): colorless solid; mp 257−260 °C; R_f = 0.15 (CH_2Cl_2); ^{1}H NMR (400 MHz, $CDCl_3$, 30 °C) δ 8.13 (s, 2H), 7.84 (d, *J* = 7.6 Hz, 2H), 7.58 (s, 2H), 7.42 (ddd, *J* = 7.6, 7.6, 1.2 Hz, 2H), 7.35−7.27 (m, 4H), 6.97 (s, 2H), 6.57 (s, 2H), 2.96 (s, 6H), 2.22 (s, 6H), 2.18 (s, 2H), 1.19 (s, 6H); ^{13}C NMR (100 MHz, $CDCl_3$, 30 °C) δ 151.6, 149.1, 138.8, 138.6, 138.4, 136.11, 136.08, 135.4, 135.0, 134.6, 132.3, 130.8, 129.2, 129.0, 124.4, 123.7, 120.9, 119.1, 85.9, 25.7, 21.7, 20.5; IR (KBr) 3542, 3403, 3010, 2968, 2918, 2857, 1633, 1609, 1548, 1567, 1490, 1476, 1451, 1421, 1380, 1324, 1289, 1264, 1200, 1173, 1152, 1120, 1099, 1043, 1006, 987, 930, 903, 894, 875, 849, 785, 754, 722, 693, 657, 634, 585, 560 cm^{-1}; MS (FAB) *m*/*z* 572.3 (M$^+$); HRMS (FAB) calcd for $C_{42}H_{36}O_2$ 572.2717, found 572.2716 (M$^+$).

*11,14-Dimesitylfluoreno[2,3-b]fluorene (**6b**).* Diol **14** (58.2 mg, 102 μmol) was placed in a Schlenk flask, and the flask was charged with Ar. After addition of toluene (20 mL), Ar was bubbled into the solution for 10 min. To this solution was added $SnCl_2$ (86.2 mg, 455 μmol), and the solution was stirred at room temperature for 2.5 h. The reaction mixture was rapidly passed through a short column on alumina (toluene) which was deactivated by water (10%) under an Ar flow to give a green fraction. After removal of the solvent under reduced pressure, recrystallization from a mixture of benzene/MeOH under an argon atmosphere gave **6b** (42.7 mg, 64%) as yellow-green crystals: mp 209 °C dec; IR (KBr) 3039, 2966, 2915, 2852, 1609, 1578, 1565, 1498, 1455, 1439, 1376, 1348, 1172, 1123, 1011, 916, 848, 768, 743, 700, 684 cm^{-1}; MS (FAB) *m*/*z* 538.4 (M$^+$); HRMS (FAB) calcd for $C_{42}H_{34}$ 538.2661, found 538.2659(M$^+$). Because of the presence of paramagnetic species, the chemical shifts of the ^{1}H NMR (Figure 4 and Figures S1 and S2) and ^{13}C NMR spectra were not recorded.

■ ASSOCIATED CONTENT

Supporting Information

The Supporting Information is available free of charge on the ACS Publications website at DOI: 10.1021/acs.joc.6b02500.

ESR spectrum for **6b**, cyclic voltammetry for **6b**, electronic absorption spectra for **6b**, NICS calculations for **6a** and **5a**, TD-DFT calculations for **6a**, comparison between experimental and theoretical values by the CASCI(2,2) method using orbitals obtained from Tuned LC-RBLYP/6-31G* calculations, and NMR spectra of **8**−**14** and **6b**, X-ray crystallographic analysis of **6b** (PDF)

X-ray crystallographic data for **6b** (CIF)

■ AUTHOR INFORMATION

Corresponding Authors

*E-mail: mnaka@cheng.es.osaka-u.ac.jp.

*E-mail: tobe@chem.es.osaka-u.ac.jp.

ORCID

Masayoshi Nakano: 0000-0002-3544-1290

Yoshito Tobe: 0000-0002-1795-5829

Present Address

#(A.S.) Department of Synthetic and Biological Chemistry, Graduate School of Engineering, Kyoto University, Kyoto 615-8510, Japan.

Notes

The authors declare no competing financial interest.

■ ACKNOWLEDGMENTS

This work was supported by JSPS KAKENHI Grant Nos. 15H02164, 15K13643, and 15J05266. M.N. expresses thanks to JSPS KAKENHI (Grant No. JP25248007 in Scientific Research (A), Grant No. JP24109002 in Scientific Research on Innovative Areas "Stimuli-Responsive Chemical Species", Grant No. JP15H00999 in Scientific Research on Innovative Areas "π-System Figuration", and Grant No. JP26107004 in Scientific Research on Innovative Areas "Photosynergetics"). We thank Prof. Y. Aso, Dr. Y. Ie, and Mr. Y. Okamoto (Institute of Science and Industrial Research, Osaka University) for the variable-temperature electronic absorption measurements. The synchrotron radiation experiments were performed at the BL38B1 of SPring-8 with the approval of the Japan Synchrotron Radiation Research Institute (JASRI) (proposal

DOI: 10.1021/acs.joc.6b02500
J. Org. Chem. 2017, 82, 1380−1388

no. 2014B1168). We are grateful to Dr. S. Baba and Dr. N. Mizuno for crystallographic data collection.

REFERENCES

(1) (a) Wu, J.; Pisula, W.; Müllen, K. *Chem. Rev.* **2007**, *107*, 718−747. (b) Iyoda, M.; Yamakawa, J.; Rahman, M. J. *Angew. Chem., Int. Ed.* **2011**, *50*, 10522−10553. (c) Narita, A.; Wang, X.-Y.; Feng, X.; Müllen, K. *Chem. Soc. Rev.* **2015**, *44*, 6616−6643. (d) Miyoshi, H.; Nobusue, S.; Shimizu, A.; Tobe, Y. *Chem. Soc. Rev.* **2015**, *44*, 6560−6577. (e) Fix, A. G.; Chase, D. T.; Haley, M. M. *Top. Curr. Chem.* **2012**, *349*, 159−195.

(2) Sun, Z.; Ye, Q.; Chi, C.; Wu, J. *Chem. Soc. Rev.* **2012**, *41*, 7857−7889.

(3) Nakano, M.; Champagne, B. *J. Phys. Chem. Lett.* **2015**, *6*, 3236−3256.

(4) Morita, Y.; Suzuki, S.; Sato, K.; Takui, T. *Nat. Chem.* **2011**, *3*, 197−204.

(5) (a) Varnavski, O.; Abeyasinghe, N.; Aragó, J.; Serrano-Pérez, J. J.; Ortí, E.; Navarrete, J. T. L.; Takimiya, K.; Casanova, D.; Casado, J.; Goodson, T. *J. Phys. Chem. Lett.* **2015**, *6*, 1375−1384. (b) Minami, T.; Nakano, M. *J. Phys. Chem. Lett.* **2012**, *3*, 145−150.

(6) (a) Abe, M. *Chem. Rev.* **2013**, *113*, 7011−7088. (b) Kubo, T. *Chem. Lett.* **2015**, *44*, 111−122.

(7) Kubo, T.; Shimizu, A.; Sakamoto, M.; Uruichi, M.; Yakushi, K.; Nakano, M.; Shiomi, D.; Sato, K.; Takui, T.; Morita, Y.; Nakasuji, K. *Angew. Chem., Int. Ed.* **2005**, *44*, 6564−6568.

(8) Umeda, R.; Hibi, D.; Miki, K.; Tobe, Y. *Org. Lett.* **2009**, *11*, 4104−4106.

(9) (a) Chase, D. T.; Rose, B. D.; McClintock, S. P.; Zakharov, L. N.; Haley, M. M. *Angew. Chem., Int. Ed.* **2011**, *50*, 1127−1130. (b) Chase, D. T.; Fix, A. G.; Rose, B. D.; Weber, C. D.; Nobusue, S.; Stockwell, C. E.; Zakharov, L. N.; Lonergan, M. C.; Haley, M. M. *Angew. Chem., Int. Ed.* **2011**, *50*, 11103−11106. (c) Chase, D. T.; Fix, A. G.; Kang, S. J.; Rose, B. D.; Weber, C. D.; Zhong, Y.; Zakharov, L. N.; Lonergan, M. C.; Nuckolls, C.; Haley, M. M. *J. Am. Chem. Soc.* **2012**, *134*, 10349−10352.

(10) Shimizu, A.; Tobe, Y. *Angew. Chem., Int. Ed.* **2011**, *50*, 6906−6910.

(11) Flynn, C. R.; Michl, J. *J. Am. Chem. Soc.* **1974**, *96*, 3280−3288.

(12) (a) Kubo, T.; Shimizu, A.; Uruichi, M.; Yakushi, K.; Nakano, M.; Shiomi, D.; Sato, K.; Takui, T.; Morita, M.; Nakasuji, K. *Org. Lett.* **2007**, *9*, 81−84. (b) Shimizu, A.; Hirao, Y.; Matsumoto, M.; Kurata, H.; Kubo, T.; Uruichi, M.; Yakushi, K. *Chem. Commun.* **2012**, *48*, 5629−5631.

(13) (a) Sun, Z.; Huang, K.-W.; Wu, J. *J. Am. Chem. Soc.* **2011**, *133*, 11896−11899. (b) Li, Y.; Heng, W.-K.; Lee, B. S.; Aratani, N.; Zafra, J. L.; Bao, N.; Lee, R.; Sung, Y. M.; Sun, Z.; Huang, K.-W.; Webster, R. D.; Navarrete, J. T. L.; Kim, D.; Osuka, A.; Casado, J.; Ding, J.; Wu, J. *J. Am. Chem. Soc.* **2012**, *134*, 14913−14922.

(14) Miyoshi, H.; Nobusue, S.; Shimizu, A.; Hisaki, I.; Miyata, M.; Tobe, Y. *Chem. Sci.* **2014**, *5*, 163−168.

(15) Hu, P.; Lee, S.; Herng, T. S.; Aratani, N.; Gonçalves, T. P.; Qi, Q.; Shi, X.; Yamada, H.; Huang, K.-W.; Ding, D.; Kim, D.; Wu, J. *J. Am. Chem. Soc.* **2016**, *138*, 1065−1077.

(16) Fukuda, K.; Nagami, T.; Fujiyoshi, J.; Nakano, M. *J. Phys. Chem. A* **2015**, *119*, 10620−10627.

(17) Rudebusch, G. E.; Zafra, J. L.; Jorner, K.; Fukuda, K.; Marshall, J. L.; Arrechea-Marcos, I.; Espejo, G. L.; Ortiz, R. P.; Gómez-García, C. J.; Zakharov, L. N.; Nakano, M.; Ottosson, H.; Casado, J.; Haley, M. M. *Nat. Chem.* **2016**, *8*, 753−759.

(18) Wright, B. B.; Platz, M. S. *J. Am. Chem. Soc.* **1983**, *105*, 628−630.

(19) Shimizu, A.; Kishi, R.; Nakano, M.; Shiomi, D.; Sato, K.; Takui, T.; Hisaki, I.; Miyata, M.; Tobe, Y. *Angew. Chem., Int. Ed.* **2013**, *52*, 6076−6079.

(20) Cooke, R. G.; Johnson, B. L.; Owen, W. R. *Aust. J. Chem.* **1960**, *13*, 256−260.

(21) Takagi, K.; Sasaki, K.; Sakakibara, Y. *Bull. Chem. Soc. Jpn.* **1991**, *64*, 1118−1121.

(22) (a) Krygowski, T. M.; Cyrański, M. *Tetrahedron* **1996**, *52*, 1713−1722. (b) Krygowski, T. M.; Cyrański, M. *Chem. Rev.* **2001**, *101*, 1385−1420.

(23) (a) Brock, C. P.; Dunitz, J. D. *Acta Crystallogr., Sect. B: Struct. Crystallogr. Cryst. Chem.* **1982**, *38*, 2218−2228. (b) Oddershede, J.; Larsen, S. *J. Phys. Chem. A* **2004**, *108*, 1057−1063. (c) Capelli, S. C.; Albinati, A.; Mason, S. A.; Willis, B. T. M. *J. Phys. Chem. A* **2006**, *110*, 11695−11703.

(24) (a) Schleyer, P. v. R.; Jiao, H.; Hommes, N. J. R. v. E.; Malkin, V. G.; Malkina, O. L. *J. Am. Chem. Soc.* **1997**, *119*, 12669−12670. (b) Schleyer, P. v. R.; Manoharan, M.; Wang, Z.-X.; Kiran, B.; Jiao, H.; Puchta, R.; Hommes, N. J. R. v. E. *Org. Lett.* **2001**, *3*, 2465−2468.

(25) (a) Ullman, E. F.; Osiecki, J. H.; Boocock, G. B.; Darcy, R. *J. Am. Chem. Soc.* **1972**, *94*, 7049−7059. (b) Eaton, S. S.; More, K. M.; Sawant, B. M.; Eaton, G. R. *J. Am. Chem. Soc.* **1983**, *105*, 6560−6567.

(26) Bleaney, B.; Bowers, K. D. *Proc. R. Soc. London, Ser. A* **1952**, *214*, 451−465.

(27) Pommerehne, J.; Vestweber, H.; Guss, W.; Mahrt, R. F.; Bässler, H.; Porsch, M.; Daub, J. *Adv. Mater.* **1995**, *7*, 551−554.

(28) Kasha, M. *J. Chem. Phys.* **1952**, *20*, 71.

(29) Anthony, J. E. *Angew. Chem., Int. Ed.* **2008**, *47*, 452−483.

(30) Bohnen, A.; Koch, K.-H.; Lüttke, W.; Müllen, K. *Angew. Chem., Int. Ed. Engl.* **1990**, *29*, 525−527.

(31) Nakano, M.; Kishi, R.; Ohta, S.; Takahashi, H.; Kubo, T.; Kamada, K.; Ohta, K.; Botek, E.; Champagne, B. *Phys. Rev. Lett.* **2007**, *99*, 033001.

(32) Yamaguchi, K. In *Self-Consistent Field: Theory and Applications*; Carbo, R., Klobukowski, M., Eds.; Elsevier: Amsterdam, 1990; pp 727−828.

(33) Tawada, Y.; Tsuneda, T.; Yanagisawa, S.; Yanai, T.; Hirao, K. *J. Chem. Phys.* **2004**, *120*, 8425−8433.

(34) Stein, T.; Eisenberg, H.; Kronik, L.; Baer, R. *Phys. Rev. Lett.* **2010**, *105*, 266802.

(35) Minami, T.; Nakano, M.; Castet, F. *J. Phys. Chem. Lett.* **2011**, *2*, 1725−1730.

(36) Das, A.; Müller, T.; Plasser, F.; Lischka, H. *J. Phys. Chem. A* **2016**, *120*, 1625−1636.

(37) Frisch, M. J.; Trucks, G. W.; Schlegel, H. B.; Scuseria, G. E.; Robb, M. A.; Cheeseman, J. R.; Scalmani, G.; Barone, V.; Mennucci, B.; Petersson, G. A.; Nakatsuji, H.; Caricato, M.; Li, X.; Hratchian, H. P.; Izmaylov, A. F.; Bloino, J.; Zheng, G.; Sonnenberg, J. L.; Hada, M.; Ehara, M.; Toyota, K.; Fukuda, R.; Hasegawa, J.; Ishida, M.; Nakajima, T.; Honda, Y.; Kitao, O.; Nakai, H.; Vreven, T.; Montgomery, J. A., Jr.; Peralta, J. E.; Ogliaro, F.; Bearpark, M.; Heyd, J. J.; Brothers, E.; Kudin, K. N.; Staroverov, V. N.; Kobayashi, R.; Normand, J.; Raghavachari, K.; Rendell, A.; Burant, J. C.; Iyengar, S. S.; Tomasi, J.; Cossi, M.; Rega, N.; Millam, J. M.; Klene, M.; Knox, J. E.; Cross, J. B.; Bakken, V.; Adamo, C.; Jaramillo, J.; Gomperts, R.; Stratmann, R. E.; Yazyev, O.; Austin, A. J.; Cammi, R.; Pomelli, C.; Ochterski, J. W.; Martin, R. L.; Morokuma, K.; Zakrzewski, V. G.; Voth, G. A.; Salvador, P.; Dannenberg, J. J.; Dapprich, S.; Daniels, A. D.; Farkas, Ö.; Foresman, J. B.; Ortiz, J. V.; Cioslowski, J.; Fox, D. J. *Gaussian 09*, Revision D.01; Gaussian, Inc., Wallingford, CT, 2009.

DOI: 10.1021/acs.joc.6b02500
J. Org. Chem. 2017, 82, 1380−1388